Chapter 5

Gaining insight in the pathophysiology of medium-chain acyl-CoA dehydrogenase deficiency by studying a mouse model

Catharina M.L. Touw[1,2,3], Karen van Eunen[2], Naomi M.E. Vink[2,3], Klary E. Niezen-Koning[2,3], Albert Gerding[2,3], Terry G.J. Derks[1,2], G. Peter A. Smit[1,2], Barbara M. Bakker[2], Dirk-Jan Reijngoud[2,3]

[1]Section of Metabolic Diseases, Beatrix Children's Hospital and [2]Center for Liver, Digestive and Metabolic Diseases, and [3]Laboratory of Metabolic Diseases, Department of Laboratory Medicine, University of Groningen, University Medical Centre of Groningen, Groningen, The Netherlands.

In preparation

ABSTRACT

Medium-chain acyl-CoA dehydrogenase (MCAD) deficiency is the most common mitochondrial fatty acid oxidation defect. Nevertheless, the pathophysiological mechanism underlying the hypoketotic hypoglycemia that is infrequently seen in patients with the disease remains to be determined. In 2005, a mouse model for MCAD deficiency was described for the first time, on a 129P2xC57BL6/J background. We subsequently crossed this mouse model back to a C57BL6/J background. This new MCAD-KO mouse model showed a considerable phenylpropionyl-CoA oxidative activity in liver homogenate and cultured skin fibroblasts, which has not been observed in cultured skin fibroblasts of patients with MCAD deficiency. However, *Acadm* gene expression and MCAD protein were absent. Prolonged fasting alone did not trigger a phenotype. Simulating MCAD deficiency in a recently published computational model of mitochondrial fatty acid oxidation showed an increased sensitivity to substrate overload as compared to the wild type condition. Differences in mitochondrial fatty acid oxidation between man and mouse make it difficult to study the pathophysiological mechanism underlying the clinical phenotype as is seen in patients with MCAD deficiency. However, by combining the knowledge that we have obtained thus far from the studies in both MCAD-KO mouse models with the latest advances in systems biology we have been able to generate a new hypothesis on a pathophysiological mechanism that may contribute to the development of the clinical phenotypes that can be seen in patients with MCAD deficiency.

INTRODUCTION

The most common mitochondrial fatty acid oxidation (mFAO) defect is medium-chain acyl-CoA dehydrogenase (MCAD) deficiency [1]. Patients with the disease can present with a life-threatening hypoketotic hypoglycemia, which can progress into coma and even sudden death. Metabolic crises occur infrequently, typically after an episode with prolonged fasting and increased metabolic stress, such as during intercurrent illness. The clinical spectrum varies considerably, ranging from neonatal death to remaining asymptomatic throughout life. Even within a group of patients with the same *ACADM* genotype, this complete clinical spectrum can be seen. As the pathophysiology of the disease remains unclear, it is currently impossible to predict which patient is at risk for the development of clinical symptoms and who is not.

In 2005, Tolwani *et al.* first described a mouse model for MCAD deficiency [2]. This mouse model was generated by inserting a vector leading to duplication of exons 8, 9, and 10, and was created on a mixed background of 129P2 and C57BL6/J strains. As a result of the inserted duplication a stop codon is introduced upon translation, leading to truncation of the MCAD monomer after exon 10. No MCAD mRNA or protein could be detected in tissues of the MCAD knock-out mice. Biochemically and clinically, this mouse model shared some characteristics with patients with the disease such as neonatal

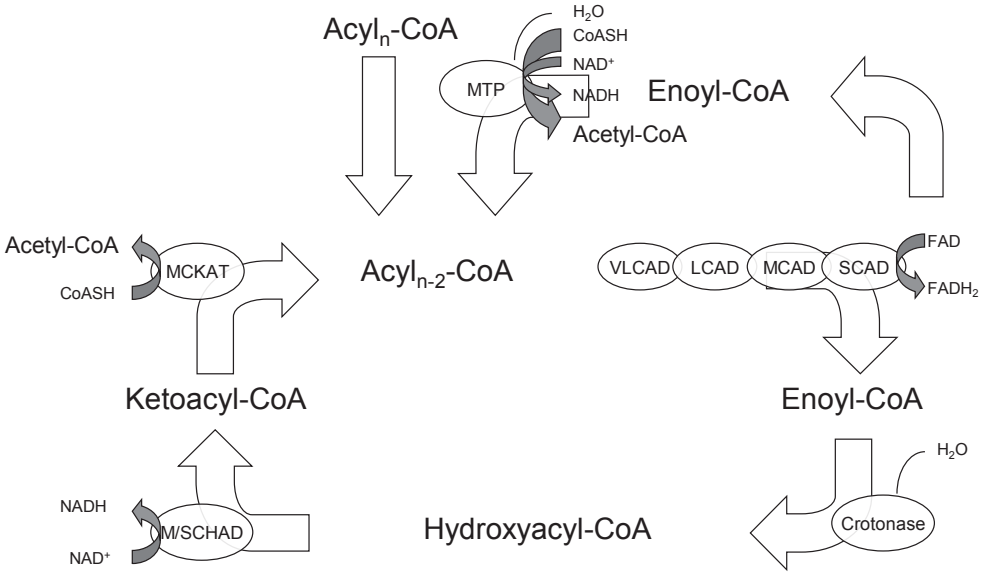

Figure 1. Schematic overview of the cyclic mFAO structure.
CoASH: Free CoA; FAD: Flavin Adenine Dinucleotide; NAD: Nicotinamide adenine dinucleotide; MCAD: Medium-chain acyl-coA dehydrogenase; MCKAT: Medium-chain ketoacyl-CoA thiolase; MSCHAD: Medium-chain hydroxyacyl-CoA dehydrogenase; MTP: Mitochondrial trifunctional protein; LCAD: Long-chain acyl-CoA dehydrogenase; LCHAD: Long-chain hydroxyacyl-CoA dehydrogenase; SCAD: Short-chain acyl-CoA dehydrogenase; SCHAD: Short-chain acyl-CoA dehydrogenase; VLCAD: Very long-chain acyl-CoA dehydrogenase.

deaths, abnormal acylcarnitine profiles, and fatty liver upon prolonged fasting. Hypoglycemia upon prolonged fasting was not observed in this mouse model. Irrespective of the absence of MCAD protein, considerable aspecific oxidative capacity has been reported in different MCAD enzyme assays: with hexanoyl-CoA as a substrate the aspecific activity was 51%, with the highly specific substrate phenylpropionyl-CoA (PP-CoA) it was 7% and in an electron transfer flavoprotein reduction assay with octanoyl-CoA the activity was 25% [2,3]. For each of these assays, observed oxidative activities were considerably higher in the mouse model than in patients [4].

Recently, we published a computational model of mFAO, which takes into account the cyclic structure of mFAO (Figure 1) and the consequent competition of acyl-CoA intermediates for the same enzymes as the original acyl-CoA substrate upon re-entering the mFAO [5]. The model was developed based on published values for the kinetic parameters of the individual enzymes for rat liver. With this model, we were able to calculate the mFAO rate, which was very close to the values measured during experimental validation in isolated rat liver mitochondria. We used this model to simulate the consequences of MCAD deficiency.

In this chapter, we describe the first results of the characterization of the backcrossed C57BL6/J MCAD-KO mouse model. Additionally, the results of the first simulations of MCAD deficiency in the computational model for mFAO will be presented.

METHODS

Mice

Regular backcrossing of MCAD-KO mice on the mixed 129P2xC57BL6/J background with the C57BL6/J strain was performed. Mice were backcrossed for 5 generations, before a subpopulation with heterozygous breeding pairs was started for the generation of MCAD-KO and wild type (WT) mice that could be used for experiments.

Genotyping of the mice occurred after weaning, and was performed with real time PCR in ear tissue, testing for a SNP only present in the inserted vector, using the following primers and probes:

Primer sequences:	Mcad-GT-Fwd: TTT GTG GTT TTC AGC GAC TAG G; Mcad-GT-Rev: GTG AAA GAT GAA CTA CAC ACA GGA CA.
Probe sequences:	Mcad-GT-WT-FAM: caa{T}{C}tc{C}{T}{C}tcca{C}c (5' 6-FAM / 3'-BHQ1); Mcad-GT-KO-YY: caa t {C}tc{C}{C}{C}tcca{C}c (5'-YY / 3'-BHQ1)).

Male mice were used for experiments at the age of 2-6 months, age variation within one experiment was never >1 month. Mice were fed commercially available laboratory chow (ABDiets, Woerden, The Netherlands).

For experiments under fasted conditions, mice were placed in a clean cage at 9 p.m. and terminated and dissected 12 hours later by cardiac puncture under isoflurane anesthesia.

All experiments were approved by the local review board for animal experiments at the University of Groningen, The Netherlands.

Metabolite analysis

Blood obtained by cardiac puncture was collected in heparinized vials. Samples were centrifuged for 10 minutes at 1200 g and 4C°. Plasma was transferred to a fresh tube and stored at -20 °C for later analysis. Free fatty acids (FFA) and β-hydroxybutyrate were determined with the Vitalab E Selectra using standard laboratory methods (reagents: DiaSys, Holzheim, Germany). Blood glucose was determined with glucose strips (One Touch® Ultra Easy, Tilburg, The Netherlands) after tail bleeding under fed and fasted conditions. Bloodspots for acylcarnitine analysis were obtained from blood obtained by cardiac puncture.

After termination, livers were dissected rapidly. One lobe of the liver was freeze clamped in liquid nitrogen and stored at -80°C until further analysis. The other part of the liver was kept fresh in sucrose buffer for oxygen uptake experiments in isolated mitochondria.

Acylcarnitines were determined in blood spots and liver homogenates under fed and fasted conditions, according to Derks *et al*.[4]

Cell culture

Skin biopsies were obtained from the ears of the mice for the isolation of fibroblasts for cell culture. Ear tags were added to culture flasks with Dulbecco's Modified Eagle Medium (DMEM) (Invitrogen), supplemented with 20% fetal bovine serum and 1.8% penicillin/streptomycin, and incubated in a 37°C 5% CO2 incubator (Steri-cycle, Thermo). Culture medium was refreshed twice a week, and the cultured skin fibroblasts were transferred to a larger culture flask when confluency was reached.

Enzyme analysis

MCAD enzyme analysis was performed in liver homogenate (n=3/group) and cultured skin fibroblasts (n=5/group). Tissues were disrupted by sonication in phosphate-buffered saline (PBS). MCAD enzyme activity was determined using phenylpropionyl-CoA as a substrate, the product cinnamoyl-CoA was measured on an HPLC system with UV detection (Waters, Milford, MA, USA) [4,6]. Residual MCAD enzyme activity was expressed as percentage of control.

Western blot analysis

The SCAD, MCAD, LCAD, and VLCAD protein levels were measured by Western blot analysis in isolated liver mitochondria (n=6/group). Isolated liver mitochondria were re-suspended in MiR05 buffer for oxygen consumption analysis (see below), and the remainder was disrupted by freezing and thawing for Western blot analysis. Protein determination was performed with a Pierce™ BCA Protein Assay Kit (Pierce Biotechnology, Inc.). For Western blot analysis, 10 µg protein was denatured, separated on a 12% SDS-page gel, and transferred onto a nitrocellulose membrane (Trans-Blot Transfer pack (Bio-Rad), 10 minutes, 25V). Blots were blocked for 1 hour with 2% ELK (Campina) powder, 0.5% BSA in PBS with 0.1% Tween-20.

The nitrocellulose membrane was immunoblotted overnight at 4°C with 1:2000 dilutions of either Anti-MCAD (Abcam, ab94261, spanning amino acid 240-290 on exon 9 and 10); Anti-SCAD (Abcam, ab156571); Anti-LCAD (Abcam, ab82853); Anti-VLCAD (Abcam, ab155138); and 1:5000 Anti-Citrate Synthase (Abcam, ab129095) for Western blot analysis on isolated liver mitochondria. Blots were then incubated for 1 hour at room temperature with 1:2000 dilution of a goat anti-rabbit polyclonal HRP secondary antibody (DakoCytomation, P0448). The Western blots were developed with SuperSignal Wester Dura Substrate (Thermo Scientific).

Quantitative PCR

Total RNA was isolated from homogenates of freeze-clamped liver tissue of adult male MCAD-KO (n=6) and WT C57BL6/J (n=6) mice using Trizol (Invitrogen, Carlsbad, CA). Quantification of total mRNA was done by NanoDrop ND-100 UV-Vis spectrophotometer (NanoDrop Technologies, Wilmington, DE, USA). cDNA was synthesized from 1 µg of total RNA according to manufacturer protocols (Invitrogen, Carlsbad, CA, USA). Real-time PCR was performed using an ABI-Prism 7700 fast PCR system (Applied Biosystems, Foster City, CA, USA). *Acadm* (spans exons 3-4, TaqMan gene expression assays, Mm01323360_g1), *Acads* (Mm00431617_m1), *Acadl* (Mm00599660_m1), and *Acadvl* (Mm00444293_m1) primers were commercially obtained (Applied Biosystems, Foster City, CA, USA). Obtained mRNA expression levels were calculated relative to the housekeeping gene 36B4, and normalized according to the mean expression levels that were obtained in the control group.

Oxygen consumption analysis

Mitochondria were isolated from livers of adult male MCAD-KO (n=6) and WT C57BL6/J mice (n=6), according to Mildaziene *et al.* [7]. The rate of oxygen consumption was measured in isolated mitochondria with palmitoyl-carnitine (C_{16}-carnitine) or octanoyl-carnitine (C_8-carnitine) as a substrate at 37°C in a stirred Oroboros oxygraph-2k (Oroboros, Innsbruck, Austria). All analyses were performed in 2 ml MiR05 buffer according to the Oroboros Instruments protocols (www.oroboros.at) [8], with 0.5 mg/ml mitochondrial protein, 2 mM malate, 1 mM ADP, 500 µM L-carnitine, 0.2 µM FCCP (uncoupler), and 25 µM of substrate.

Calculation of rate of oxygen consumption due to the mFAO

The measured oxygen consumption is not directly related to C_{16}-carnitine oxidation in the presence of malate. Malate was added to the medium to enable regeneration of CoASH from acetyl-CoA by reaction (1):

$$\text{Acetyl-CoA} + \text{Oxaloacetate} + H_2O \longleftrightarrow \text{Citrate} + \text{CoASH} + H^+ \qquad \text{(reaction 1)}$$

In this reaction oxaloacetate is generated by malate oxidation. As a consequence, the oxygen consumption during C_{16}-carnitine oxidation is the sum of malate oxidation (1/3 of measured oxygen consumption) and β-oxidation (2/3 of measured oxygen consumption).

Modeling MCAD deficiency

MCAD deficiency was simulated in the dynamic model of the mFAO as previously described by van Eunen *et al.* [5]. In our model we used experimentally determined kinetic parameters of the involved enzymes published for rat liver. The model outcome was experimentally validated in isolated rat liver mitochondria, and was found to qualitatively predict metabolite concentrations and rates in time without prior parameter estimation. In contrast to the two other computational models that had previously been reported for mFAO, our model takes into account the complex interactions and competitions that take place in the pathway as a consequence of its cyclic nature and the overlap in substrate specificity of the enzymes involved [5,9,10]. In order to model MCAD deficiency, the V_{max} for liver MCAD was adapted to 10% of control values, which corresponded to the average aspecific oxidative activity for PP-CoA oxidation observed in the MCAD-KO mouse model.

Statistical analysis

Dichotomous data were analyzed with a chi-squared test. Differences between normally distributed continuous data were analyzed using parametric tests, and data that were not normally distributed were analyzed using non-parametric tests. The significance level was set at $p<0.05$. Statistical analyses were performed using GraphPad Prism software (GraphPad Software Inc., version 5.00, 2007).

RESULTS

Mouse characteristics

Neonatal deaths as seen in the 129P2xC57BL6/J MCAD-KO strain were not observed in the heterozygous breeding program of the C57BL6/J MCAD+/- mice (upon weaning 339 pups: 73 MCAD-KO (22%), 176 MCAD+/- (51%), 90 WT (27%); chi-square with Mendelian inheritance as null hypothesis, $p=0.45$). Body weight under fed and fasted conditions was similar in the MCAD-KO and WT group. Loss of body weight and the liver/body weight ratio upon fasting were also similar in both groups (Table 1). Concentrations of blood glucose, free fatty acids, and β-hydroxybutyrate were similar in the MCAD-KO group and the control group after 12 hours of fasting (Table 1). C_6-, C_8-, and $C_{10:1}$-carnitine, and the C_8/C_{10} ratio were significantly higher in bloodspots of the C57BL6/J MCAD-KO mice under these same conditions ($p<0.01$, Table 1).

Medium-chain acylcarnitine concentrations in liver homogenate fed and fasted

Acylcarnitine profiles in liver homogenates of fed and 12-hour fasted mice showed remarkable results. Under fed conditions, concentrations of C_6-, C_8-, C_{10}-, and $C_{10:1}$-carnitine were similar in the MCAD-KO and the WT group. Upon a 12-hour fast C_6- and C_8-carnitine remained similar in the MCAD-KO group when compared to fed conditions, whereas concentrations of C_{10}- and $C_{10:1}$-carnitine increased (Table 2). In the WT group, concentrations of C_6-carnitine appeared to decrease; however, this effect did not reach statistical significance. Concentrations of C_{10}-carnitine increased significantly. Concentrations of

Table 1: Mouse characteristics after a 12-hour fast

	MCAD-KO	WT
Fasted body weight (g)	23.0 (20.7-27.1)	23.9 (17.8-27.1)
Body weight loss upon fasting (%)	11.2 (10.0-13.8)	12.4 (7.8-19.9)
Body weight/liver ratio	0.050 (0.041-0.053)	0.047 (0.043-0.052)
Fasted glucose (mmol/l)	5.3 (4.6-6.8)	5.8 (4.6-7.8)
Fasted β-OH-butyrate (mmol/l)‡	1.35 (1.29 – 1.99)	2.30 (1.59 – 2.60)
Free fatty acids (mmol/l) ‡	583 (516 – 598)	432 (410 – 714)
C_6-carnitine bloodspot (µmol/l)	0.14 (0.09 – 0.30)**	0.06 (0.04 – 0.07)
C_8-carnitine bloodspot (µmol/l)	0.49 (0.46 – 0.56)**	0.07 (0.06 – 0.42)
C_8/C_{10} ratio bloodspot	7.6 (5.3 – 9.3)**	3.2 (2.4 – 6.9)
C_{10}-carnitine bloodspot (µmol/l) ‡	0.07 (0.05 – 0.09)	0.03 (0.02 – 0.06)
$C_{10:1}$-carnitine bloodspot (µmol/l) ‡	0.22 (0.10 – 0.26)**	0.02 (0.01 – 0.02)

Median and range are depicted. ‡ Blood samples of two mice were pooled for this analysis. Three pooled plasma samples were analyzed per genotype. ** $p<0.01$.

the other medium-chain acylcarnitines did not change in this group upon fasting. Fasting concentrations of C_6-, C_{10}- and $C_{10:1}$-carnitine were significantly higher in the C57BL6/J MCAD-KO group when compared to the WT group upon fasting.

Enzyme activity

Analysis of the MCAD enzyme activity with PP-CoA in liver homogenate resulted in a median PP-CoA oxidation activity of 9.3% (n=3, range 9.0-11.2%) when compared to control. These results were comparable to activities that were previously measured in the 129P2xC57BL6/J MCAD-KO strain [3]. In cultured skin fibroblasts of the same mouse strains a median PP-CoA oxidation activity of 10.9% (n=5, range 9.8-19.6%) of control was found.

Western blot analysis

No MCAD protein was detected upon Western blot analysis in isolated liver mitochondria of MCAD-KO mice (Figure 2A, B). The amount of SCAD, LCAD, and VLCAD protein detected upon prolonged fasting was similar in the MCAD-KO and WT group.

Table 2. Concentrations of medium-chain acylcarnitines in liver homogenate under fed and fasted conditions.

		FED	FASTED
		n=5	n=6
MCAD-KO	C_6	0.52 (0.42 – 0.54)	0.52 # (0.48 – 0.64)
	C_8	0.06 (0.04 – 0.10)	0.07 (0.06 – 0.08)
	C_{10}	0.06 (0.04 – 0.08)	0.29 *# (0.10 – 0.38)
	$C_{10:1}$	0.00 (0.00 – 0.02)	0.04 *# (0.02 – 0.06)
		n=6	n=5
WT	C_6	0.50 (0.40 – 0.64)	0.40 # (0.40 – 0.50)
	C_8	0.06 (0.04 – 0.08)	0.08 (0.04 – 0.12)
	C_{10}	0.06 (0.02 – 0.06)	0.12 *# (0.08 – 0.14)
	$C_{10:1}$	0.00 (0.00 – 0.02)	0.02 # (0.00 – 0.04)

Concentrations in µmol/l. * significantly different from fed conditions (p<0.05); # significantly different from other fasted group (p<0.05). Mice in the 'fasting' group were fasted for 12 hours.

Quantitative PCR

Acadm mRNA was almost absent in liver homogenate of MCAD-KO mice. Expression of *Acads, Acadl,* and *Acadvl* upon prolonged fasting was similar in the MCAD-KO and WT group (Figure 3).

Oxygen consumption rate

Analysis of the rate of oxygen consumption in isolated liver mitochondria of fed mice determined similar oxygen consumption rates in the MCAD-KO mouse when compared to the WT group (median 43.8 nmol/min/mg protein vs. 55.0 nmol/min/mg protein respectively) when C_{16}-carnitine was used as a substrate (Figure 4A). When C_8-carnitine was used as a substrate, median maximum rate in the MCAD-KO mice was 50% of the median maximum rate that was observed in the WT group (median 29.0 nmol/min/mg protein vs. 58.4 nmol/min/mg protein respectively, p<0.001)(Figure 4B).

Modeling MCAD deficiency

Our computational model of mFAO [5] predicted that the cyclic structure and the overlapping substrate specificity of the enzymes involved makes mFAO susceptible for substrate overload. After one cycle of mFAO the shortened acyl-CoAs will re-enter the mFAO cycle for further oxidation. They thereby compete with other intermediates and newly entering acyl-CoAs for the same enzymes in the oxidative pathway (Figure 1). This competition leads to feedforward inhibition, with subsequent accumulation

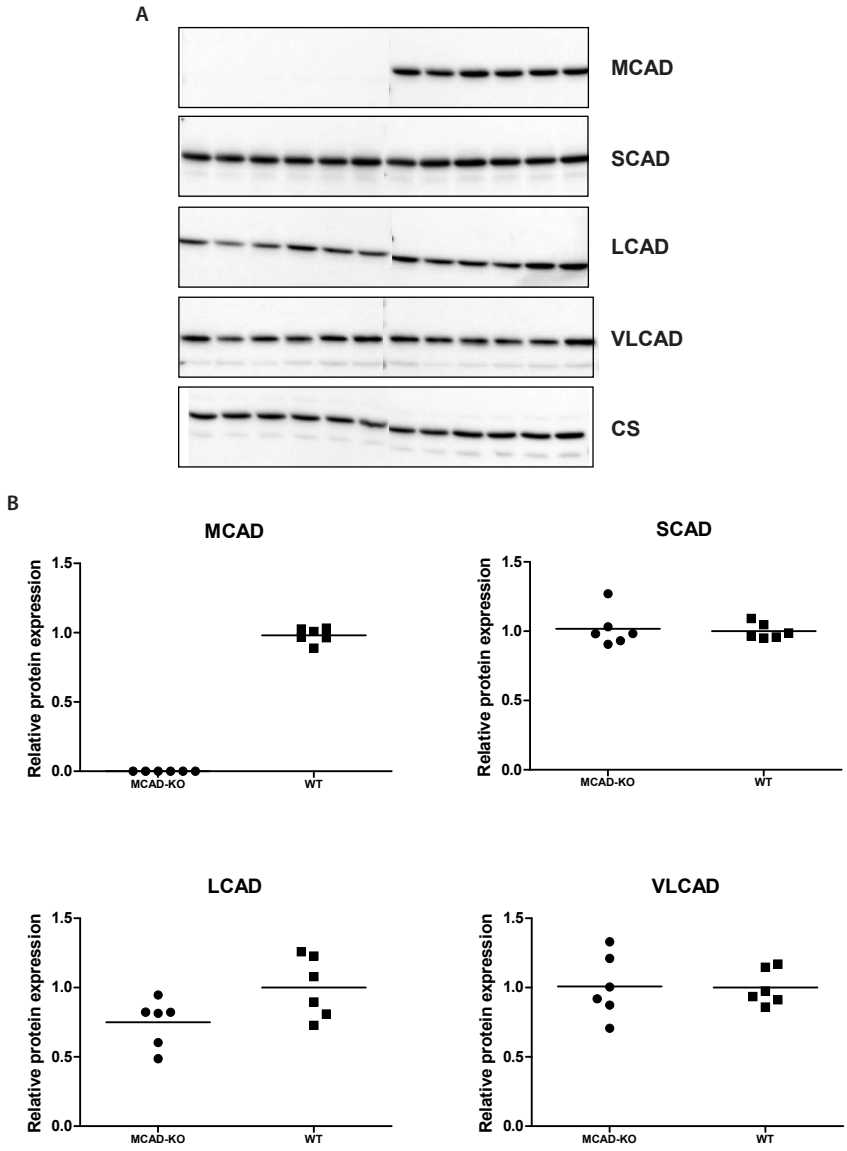

Figure 2. Western blot of MCAD, SCAD, LCAD, VLCAD, and citrate synthase protein in isolated liver mitochondria of fasted mice (A). CS: Citrate synthase. Quantification occurred according to the housekeeping gene. Mean relative protein expression in the WT group was set at 1. Relative protein expression in all animals was related to the mean relative protein expression in the WT group (B).

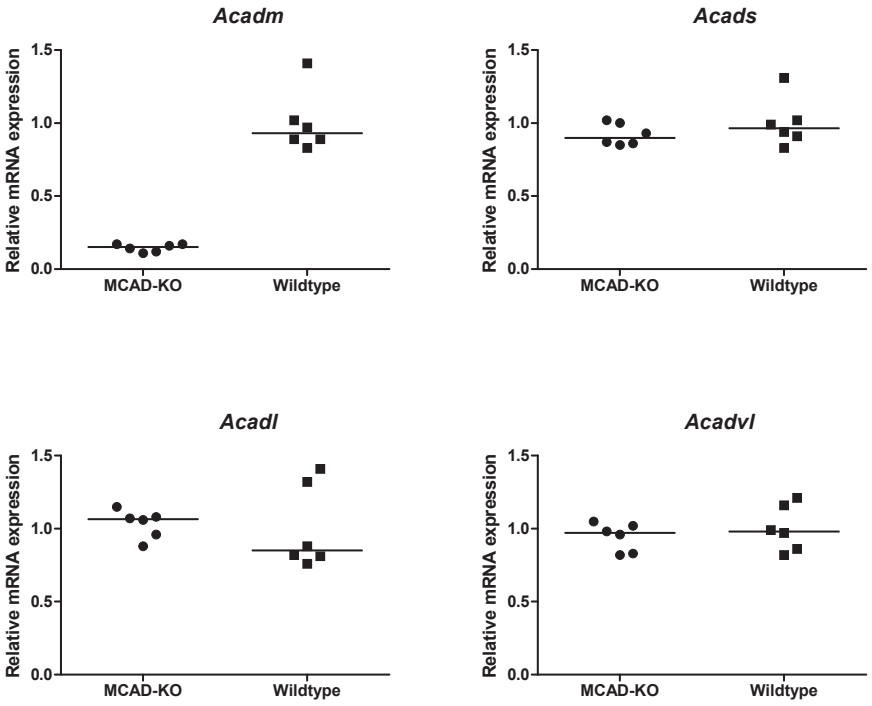

Figure 3. Relative mRNA expression of *Acadm, Acads, Acadl,* and *Acadvl* in liver homogenate of fasted C57BL6/J MCAD-KO and WT mice. *Acadm*: Gene encoding MCAD; *Acads*: Gene encoding SCAD; *Acadl*: Gene encoding LCAD; *Acadvl*: Gene encoding VLCAD. Mean gene expression per group is indicated.

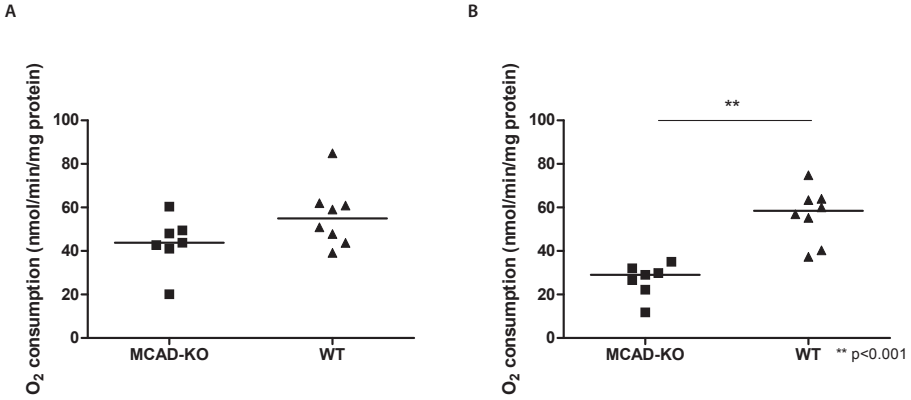

Figure 4. Oxygen consumption rate measured in oxygraph in isolated liver mitochondria, with C_{16}-carnitine (A) and C_8-carnitine (B) as substrates. The total oxygen consumption (of which 1/3 can be attributed to malate dehydrogenase activity, and 2/3 to the β-oxidation) is depicted. Oxygen consumption in nmol/min/mg protein. ** $p<0.001$.

of acyl-CoA esters and depletion of CoASH [5]. Based on the outcome of these model simulations we wondered if MCAD deficiency makes our model of mFAO even more vulnerable to substrate overload. To simulate MCAD deficiency, V_{max} of MCAD was set at 10% of normal. The MCAD deficient model showed accumulation of medium-chain acylcarnitines upon simulation of C_{16}-CoA oxidation, which showed similarities to the acylcarnitine profiles that were observed in liver homogenate of the fed MCAD-KO mouse model. C_6-carnitine was the predominant metabolite, followed by respectively C_8-carnitine and C_{10}-carnitine (Figure 5A). We then performed a series of simulations to mimic substrate overload (Figures 5B, C). In the unperturbed model, in which the V_{max} of MCAD was kept at 100% of normal (WT), we increased the concentrations of C_{16}-CoA in a stepwise manner and calculated the steady-state rate (i.e. flow) through mFAO. At a concentration of 50 μM of C_{16}-CoA the WT rate through the β-oxidation dropped abruptly (Figure 5B) with a concomitant rapid increase in the concentration of various acyl-CoA intermediates and a pronounced decrease in CoASH concentration (Figure 5C). When the same series of simulations were performed in the MCAD deficient model, a sudden drop in rate occurred already at a much lower concentration of C_{16}-CoA (approximately 10 μM), accompanied by comparable changes in the concentration of mFAO intermediates and CoASH as observed in the WT simulations, albeit at lower concentrations of C_{16}-CoA (Figure 5B). Quite strikingly, close inspection

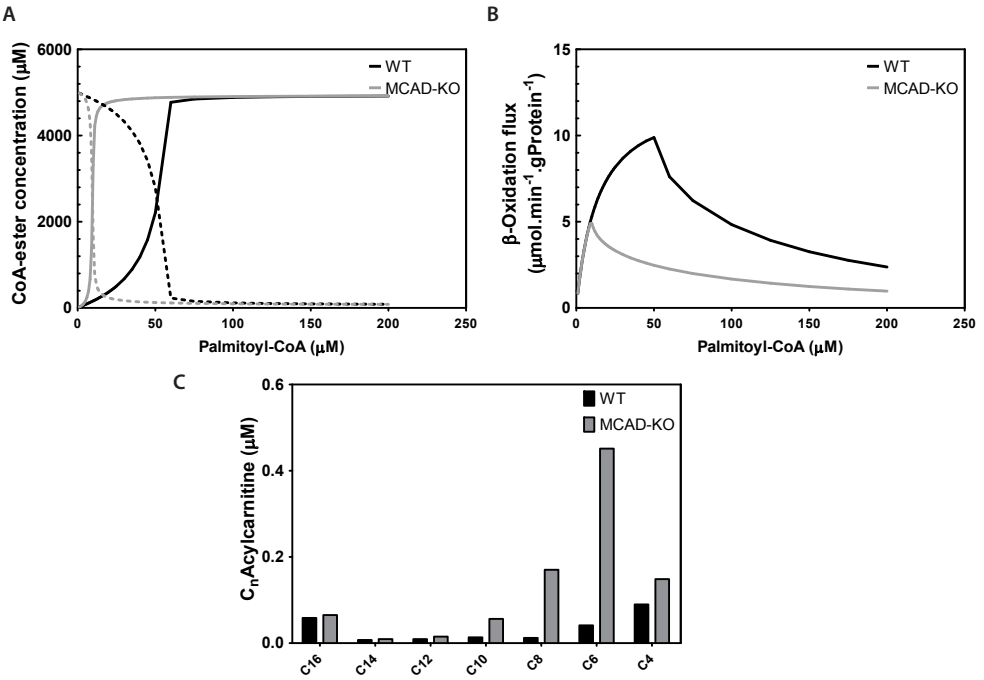

Figure 5. Acylcarnitine concentrations (A), steady-state oxygen consumption rate through the β-oxidation (B), and acyl-CoA ester concentrations (C) in a computational model for MCAD deficiency. Black bars and lines: Wild type situation; Grey bars and lines: MCAD-KO situation (V_{max} 10% of control). Figure A: Solid lines, Acyl-CoA ester concentrations; dotted lines, CoASH concentrations.

of the outcome of these model simulations revealed that the predicted rates of oxidation of C_{16}-CoA were the same in both models up to the point where substrate overload became manifest in the MCAD deficient model. Our simulations predicted that the decreased ability to oxidize fatty acids in the case of MCAD deficiency was due to substrate overload instead of a proportionally decreased rate of oxidation at all concentrations of C_{16}-CoA.

DISCUSSION

We present a first characterization of the MCAD-KO mouse model on a C57BL6/J background. Furthermore, we applied our dynamic model of mFAO to simulate MCAD deficiency. Characterization of the MCAD-KO C57BL6/J mouse led to similar results as were reported in the MCAD-KO 129P2xC57BL6/J mouse model [2,3]. On a C57BL6/J background, the MCAD-KO mice showed acylcarnitine profiles in bloodspots similar to those observed in MCAD deficient patients, even though profiles were slightly different in liver homogenate, where C_6-carnitine was the predominant metabolite. Aspecific oxidative capacity measured in frozen liver homogenate of C57BL6/J MCAD-KO mice with PP-CoA showed almost 10% of capacities observed in C57BL6/J WT mice, considerably higher than what is generally observed in MCAD deficient patients (<1% of control). Oxygen consumption upon administration of C_8- and C_{16}-carnitine showed characteristics of MCAD deficiency. Introducing MCAD deficiency in our dynamic model of mFAO predicted almost equal C_{16}-CoA steady-state rate in the MCAD deficiency model when compared to the unperturbed WT model at low concentrations of the substrate. However, the outcome of our predictions showed an increased vulnerability for substrate overload in the case of the MCAD deficiency model.

Phenotypically the mouse model did not show the full clinical spectrum that has been described in human patients. We did not observe neonatal deaths when breeding these mice heterozygously, and these mice did not develop hypoketotic hypoglycemia upon prolonged fasting alone. Although remaining asymptomatic is a 'phenotype' that we often observe in patients with MCAD deficiency, in the C57BL6/J MCAD-KO mouse model we did not observe the other, potentially lethal, end of the spectrum as can be seen in patients. This may correspond to the considerable PP-CoA oxidation activity that was observed in cultured skin fibroblasts of this mouse model (~10% of WT activity), but not in patients with classical *ACADM* genotypes (<1% of normal). However, the origin of this PP-CoA oxidative activity in the MCAD-KO mouse is unclear, as PP-CoA is thought to be specifically oxidized by MCAD, at least in rat and human liver tissue [11]. Moreover, this aspecific oxidative activity was not found to be liver specific.

Besides residual PP-CoA oxidative activities, observed activities for C_6-CoA and C_8-CoA oxidation in C57BL6/J MCAD-KO mice were considerably higher than activities measured in patients with *ACADM* genotypes that are associated with the risk to develop a metabolic crisis [2,3]. These differences may be attributable to differences in chain length specificities and kinetic parameters of the various mFAO enzymes between humans and rodents. For instance, in rodents long-chain acyl-CoA dehydrogenase

(LCAD) participates in mFAO, whereas in humans LCAD plays only a minor role in saturated fatty acid oxidation, and is hardly expressed [12]. As rodent LCAD displays a considerable activity towards C_8-CoA, this enzyme may play an important role in substrate dehydrogenation and thereby partially compensate for the absent MCAD enzyme in MCAD-KO mice [13]. Adaptations to defective mFAO by upregulation of other acyl-CoA dehydrogenases has been described in the mouse model for very long-chain acyl-CoA dehydrogenase (VLCAD) deficiency [14]. However, analysis of LCAD protein and mRNA expression in both liver homogenate and cultured skin fibroblasts showed no differences between MCAD-KO mice and WT mice. Compensation for the defect by LCAD could therefore not be established in the C57BL6/J MCAD-KO mouse model, although we did not measure LCAD activity, which is modified by post-translational modification [15]. The origin of the aspecific oxidative capacity of C_6-CoA, C_8-CoA, and PP-CoA remains unknown.

Remarkable acylcarnitine profiles were observed in liver homogenates of MCAD-KO mice under both fed and fasted conditions. The acylcarnitine profiles that we observed in liver homogenate of MCAD-KO and WT mice, and its response to fasting, may include activated lipogenesis under fed conditions [16]. It has previously been shown that lipogenetic fatty acids can be recovered in acylcarnitines in the circulation. ^{13}C-label of short-chain fatty acids could be recovered in C_{16}-carnitine [17]. These findings may indicate that in MCAD-KO mice, a similar phenomenon occurs under fed conditions. However, under fasted conditions, concentrations of medium-chain acylcarnitines were significantly higher in MCAD-KO mice when compared to WT mice. Upon prolonged fasting, high concentrations of triacylglycerols are released from adipose tissue, for the generation of free fatty acids that can undergo β-oxidation in the liver [18]. As mFAO is activated during fasting, the load of medium-chain length acyl-CoA esters and acylcarnitines increases under MCAD-deficient conditions. As lipogenesis is inhibited upon fasting [19], it may not be sufficient for the prevention of accumulation of medium-chain length acylcarnitines.

When the oxidation of C_{16}-carnitine was measured in isolated liver mitochondria of MCAD-KO mice we observed an almost normal rate of oxygen uptake. Oxidation of C_8-carnitine was 50% of normal, by itself a remarkable observation, because of the complete absence of the MCAD enzyme. Apparently, other enzymes are also active in oxidizing C_8-carnitine. If we look more closely at the way β-oxidation proceeds, an almost normal oxidation rate of C_{16}-carnitine in isolated liver mitochondria of MCAD-KO mice can be explained. Oxidation of C_{16}-carnitine to C_8-CoA in MCAD deficiency leads to the production of 4 acetyl-CoA units at a rate which can be normal, when intermediate acyl-CoAs do not perturb the rate through the β-oxidation. When it is assumed that the next 4 acetyl-CoA units, from C_8-CoA to acetyl-CoA, will be produced at 50% of the normal rate, irrespective of the actual concentration of C_8-CoA during C_{16}-carnitine oxidation, the overall rate of oxygen consumption during C_{16}-carnitine oxidation would only be decreased to 75% of the value observed in isolated liver mitochondria of WT mice.

In the past decade, the application of systems biology in medical research has grown steadily with the development of computational models for glucose metabolism [20,21], the TCA cycle [22], and mFAO [5]. We recently published a new dynamic model for mFAO incorporating competition between short-

ened products and the original substrate acyl-CoAs due to the cyclic nature of mFAO. We predicted that this competition would make mFAO vulnerable to substrate overload. This led us to hypothesize that mFAO defects may increase this vulnerability even further. We simulated mFAO of C_{16}-CoA when the V_{max} for MCAD enzyme activity was reduced to 10% of the value we normally used in the model for rat liver. The simulation showed an enhanced vulnerability to substrate overload of mFAO when MCAD activity was impaired when compared to the WT situation. Already at low concentrations of C_{16}-CoA the simulations predicted an abrupt drop in the rate through mFAO, indicative for substrate overload. The model also predicted that until the point of substrate overload was reached, the rate through mFAO in the presence of MCAD insufficiency was almost indistinguishable from the rate in the presence of a normal value for the V_{max} of MCAD. This might indicate that the rate through mFAO with an MCAD V_{max} of 10% of WT might be normal, irrespective of impaired MCAD activity. If mFAO in MCAD-KO mice truly has an almost normal activity, acute inhibition of mFAO during metabolic crises in MCAD deficient patients might be the consequence of substrate overload only. When it occurs depends on the capacity of oxidative phosphorylation, and the ability to dissipate the excess acyl-CoAs into pathways such as lipogenesis and acylcarnitine formation, thereby preventing substrate overload.

Administration of L-carnitine may both stimulate and inhibit the development of substrate overload. First of all, it can aid in the disposal of acyl-CoAs by conversion to acylcarnitines. On the other hand, it may also drive the mitochondrial entry of acyl-CoAs, especially in case of increased energy demands, thereby increasing the susceptibility of mFAO for substrate overload. Studies hereon are lacking in patients with mFAO defects.

Patients might also become more vulnerable to metabolic crises when delivery of dicarboxylic acids to the liver by gut microbial metabolism is combined with heightened energy demand from mFAO. This may occur during intercurrent illness and in particular during a gastrointestinal infection. Many of the dicarboxylic acids are oxidized by the concerted action of a ligase followed by MCAD. As a result, sensitivity to substrate overload may even be further increased. If this is the case, and substrate overload is a purely acute hepatic metabolic process, it indicates that no trace of the decompensation of the patient is left after the metabolic crises has resolved. It should however be noted that this outcome is based on simulations in an isolated model of mFAO in rat liver. Adaptations to render this model useful for studying mouse metabolism and integration of mFAO in total mitochondrial metabolism in detail are ongoing. Finally, the translation to the human situation has to be made.

CONCLUSIONS

In conclusion, differences in mFAO between mouse and human make it difficult to study pathophysiological mechanisms contributing to the development of the clinical phenotype as is infrequently seen in patients with MCAD deficiency. Not only is the residual activity towards PP-CoA, C_6-CoA, and C_8-CoA oxidation higher in the mouse model than in patients, concentrations of accumulating inter-

mediates and their chain-length also differ slightly from the acylcarnitine profiles that are usually seen in patients. The possible role of peroxisomes and microsomes in compensating for the MCAD defect remains to be elucidated [23]. Additionally, approaches studying the possibility of substrate overload, as predicted by our dynamic model of mFAO are required to obtain insight in factors that determine the risk for a metabolic crisis. Once the pathophysiological mechanisms contributing to the development of a hypoketotic hypoglycemia have been unraveled, studies on therapeutic options can be initiated.

REFERENCES

1. Roe CR, Ding J. Chapter 101: Mitochondrial fatty acid oxidation disorders. In: Valle D, Scriver CR, editors. The online metabolic and molecular bases of inherited disease. 8th ed. New York: McGraw-Hill; 2001.
2. Tolwani RJ, Hamm DA, Tian L, et al. Medium-chain acyl-CoA dehydrogenase deficiency in gene-targeted mice. *PLoS Genet* 2005; **1**(2): e23.
3. Herrema H, Derks TG, van Dijk TH, et al. Disturbed hepatic carbohydrate management during high metabolic demand in medium-chain acyl-CoA dehydrogenase (MCAD)-deficient mice. *Hepatology* 2008; **47**(6): 1894-904.
4. Derks TG, Boer TS, van Assen A, et al. Neonatal screening for medium-chain acyl-CoA dehydrogenase (MCAD) deficiency in The Netherlands: the importance of enzyme analysis to ascertain true MCAD deficiency. *J Inherit Metab Dis* 2008; **31**(1): 88-96.
5. van Eunen K, Simons SMJ, Gerding A, et al. Biochemical competition makes fatty-acid beta-oxidation vulnerable to substrate overload. *PLOS Computational Biology* 2013; **9**(8): e1003186.
6. Wanders RJ, Ruiter JP, IJLst L, Waterham HR, Houten SM. The enzymology of mitochondrial fatty acid beta-oxidation and its application to follow-up analysis of positive neonatal screening results. *J Inherit Metab Dis* 2010; **33**(5): 479-94.
7. Mildaziene V, Nauciene Z, Baniene R, Grigiene J. Multiple effects of 2,2',5,5'-tetrachlorobiphenyl on oxidative phosphorylation in rat liver mitochondria. *Toxicol Sci* 2002; **65**(2): 220-7.
8. Gnaiger E, Kuznetsov A, Schneeberger S, Seiler R, Brandacher G, Steurer W, Margreiter R. Mitochondria in the cold. In: Heldmeier G, Klingenspor M, editors. Life in the Cold. Springer; 2000. p.431.
9. Kohn MC, Garfinkel D. Computer simulation of metabolism in palmitate-perfused rat heart. I. Palmitate oxidation. *Ann Biomed Eng* 1983; **11**(5): 361-84.
10. Modre-Osprian R, Osprian I, Tilg B, Schreier G, Weinberger KM, Graber A. Dynamic simulations on the mitochondrial fatty acid beta-oxidation network. *BMC Syst Biol* 2009; **3**: 2,0509-3-2.
11. Rinaldo P, O'Shea JJ, Welch RD, Tanaka K. The enzymatic basis for the dehydrogenation of 3-phenylpropionic acid: in vitro reaction of 3-phenylpropionyl-CoA with various acyl-CoA dehydrogenases. *Pediatr Res* 1990; **27**(5): 501-7.
12. Maher AC, Mohsen AW, Vockley J, Tarnopolsky MA. Low expression of long-chain acyl-CoA dehydrogenase in human skeletal muscle. *Mol Genet Metab* 2010; **100**(2): 163-7.
13. Wanders RJ, Vreken P, den Boer ME, Wijburg FA, van Gennip AH, IJlst L. Disorders of mitochondrial fatty acyl-CoA beta-oxidation. *J Inherit Metab Dis* 1999; **22**(4): 442-87.
14. Tucci S, Herebian D, Sturm M, Seibt A, Spiekerkoetter U. Tissue-specific strategies of the very-long chain acyl-CoA dehydrogenase-deficient (VLCAD-/-) mouse to compensate a defective fatty acid beta-oxidation. *PLoS One* 2012; **7**(9): e45429.
15. Hirschey MD, Shimazu T, Goetzman E, et al. SIRT3 regulates mitochondrial fatty-acid oxidation by reversible enzyme deacetylation. *Nature* 2010; **464**(7285): 121-5.
16. Nugteren DH. The enzymic chain elongation of fatty acids by rat-liver microsomes. *Biochim Biophys Acta* 1965; **106**(2): 280-90.
17. den Besten G, Lange K, Havinga R, et al. Gut-derived short-chain fatty acids are vividly assimilated into host carbohydrates and lipids. *Am J Physiol Gastrointest Liver Physiol* 2013; .
18. Kersten S, Seydoux J, Peters JM, Gonzalez FJ, Desvergne B, Wahli W. Peroxisome proliferator-activated receptor alpha mediates the adaptive response to fasting. *J Clin Invest* 1999; **103**(11): 1489-98.
19. Kersten S. Mechanisms of nutritional and hormonal regulation of lipogenesis. *EMBO Rep* 2001; **2**(4): 282-6.

20. Lambeth MJ, Kushmerick MJ. A computational model for glycogenolysis in skeletal muscle. *Ann Biomed Eng* 2002; **30**(6): 808-27.
21. Konig M, Bulik S, Holzhutter HG. Quantifying the contribution of the liver to glucose homeostasis: a detailed kinetic model of human hepatic glucose metabolism. *PLoS Comput Biol* 2012; **8**(6): e1002577.
22. Wu F, Yang F, Vinnakota KC, Beard DA. Computer modeling of mitochondrial tricarboxylic acid cycle, oxidative phosphorylation, metabolite transport, and electrophysiology. *J Biol Chem* 2007; **282**(34): 24525-37.
23. Violante S, Ijlst L, Te Brinke H, et al. Peroxisomes contribute to the acylcarnitine production when the carnitine shuttle is deficient. *Biochim Biophys Acta* 2013; **1831**(9): 1467-74.